# Nanostructures: Scattering beyond the Born approximation

S. V. Grigoriev,[1] A. V. Syromyatnikov,[1,2] A. P. Chumakov,[1] N. A. Grigoryeva,[2] K. S. Napolskii,[3] I. V. Roslyakov,[3] A. A. Eliseev,[3] A. V. Petukhov,[4] and H. Eckerlebe[5]

[1]*Petersburg Nuclear Physics Institute, Gatchina, 188350 St. Petersburg, Russia*

[2]*Faculty of Physics, St. Petersburg State University, 198504 St. Petersburg, Russia*

[3]*Department of Materials Science, Moscow State University, 119992 Moscow, Russia*

[4]*van 't Hoff Laboratory, Debye Institute for Nanomaterials, University of Utrecht, The Netherlands*

[5]*GKSS Forschungszentrum, 21502 Geesthacht, Germany*

(Received 24 October 2009; revised manuscript received 22 January 2010; published 4 March 2010)

The neutron scattering on a two-dimensional ordered nanostructure with the third nonperiodic dimension can go beyond the Born approximation. In our model supported by the exact theoretical solution a well-correlated hexagonal porous structure of anodic aluminum oxide films acts as a peculiar two-dimensional grating for the coherent neutron wave. The thickness of the film $L$ (length of pores) plays important role in the transition from the weak to the strong scattering regimes. It is shown that the coherency of the standard small-angle neutron scattering setups suits to the geometry of the studied objects and often affects the intensity of scattering. The proposed theoretical solution can be applied in the small-angle neutron diffraction experiments with flux lines in superconductors, periodic arrays of magnetic or superconducting nanowires, as well as in small-angle diffraction experiments on synchrotron radiation.

DOI: 10.1103/PhysRevB.81.125405 PACS number(s): 61.05.fg, 61.46.−w, 62.23.St

## I. INTRODUCTION

The present exceptional growth in the production of periodic nanostructure arrays requires both to develop characterization tools and to reconsider established tools. Until recently, most users applied the techniques of small-angle neutron scattering (SANS) and small-angle x-ray scattering (SAXS) to study the disordered state of matter at nanoscale. A periodicity in the structure will transform diffuse scattering into Bragg diffraction with its characteristic peaks. The naive expectation that small-angle diffraction on periodic nanostructure arrays should be similar to diffraction on structures of atomic scale is sometimes incorrect. The reason is that the size of the building blocks in nanostructures is much larger than the size of atomic structures, so the former in general produce much stronger scattering. One can therefore expect that diffraction on nanostructures will easier deviate from the weak scattering regime, as described by the Rayleigh-Gans theory in optics and the Born approximation in quantum mechanics.

Diffraction on two-dimensional periodic structures with a nonperiodic large third dimension is of special interest. As an example we take anodic aluminum oxide (AAO) that has recently attracted close attention of researchers, in view of the development of a two-step anodic oxidation method which opens the possibility to produce high-quality AAO films with a self-ordered porous structure.[1] AAO films are now most widely used as matrices to prepare ordered arrays of one-dimensional nanostructures of various compositions.[2,3] The most popular methods for studying the self-organization of pores during the anodization process are scanning electron microscopy and atomic force microscopy,[4–7] which, however, can address only surface structure and only within a limited area. Although the methods of SANS and SAXS were extensively used to study other spatially ordered materials, little attention has been paid to AAO membranes and AAO-based nanocomposites. At the same time these methods can provide extremely valuable information on a porous structure (interpore distance, pore diameter, and length) and their organization (positional correlation length, domain size, and mosaicity).[8]

In this paper, we show that the SANS patterns from AAO membranes display an unusual behavior, which indicates a deviation from the Born approximation. We give an exact theoretical description of neutron diffraction from such nanostructures, both within and beyond the Born approximation. We discuss to what extent the theory can be applied in the condition of a SANS experiment with limited resolution. Furthermore, we argue that a similar behavior can be found in a wide range of systems: from colloidal crystals[9–13] to Abrikosov's flux lines in superconductors.[14–16]

The manuscript is organized in the usual way. Section II gives the description of the AAO samples and details of the experimental SANS setup. Section III provides the theoretical description of neutron scattering on AAO and a discussion of the resolution limitations of the SANS experiment. Section IV presents the experimental results and gives their comprehensive interpretation. Section V concludes the manuscript.

## II. EXPERIMENTAL

$Al_2O_3$ films with a highly ordered porous structure were synthesized following a two-step anodization technique.[17,18] Prior to anodization, high purity aluminum plates (99.999%, 0.5 mm thick, Goodfellow) were annealed at 550 C for 24 h in air in order to remove the mechanical stress and to enhance the grain size in the metal. Subsequently, the Al plates were mechanically polished to a mirror finish, cleaned with acetone and deionized water in ultrasound waves, and subjected to anodization. A first anodization step was carried out in a two-electrode cell in 0.3M $(COOH)_2$ (98%, Aldrich) at a

 

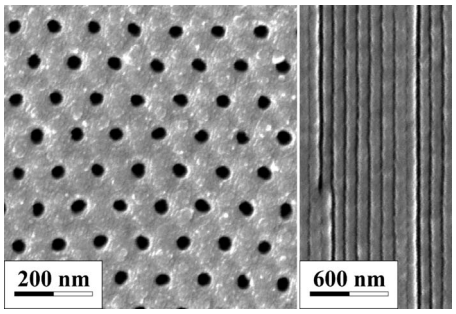


FIG. 1. SEM image of AAO membrane synthesized in 0.3M $(COOH)_2$ at 40 V: left panel—top view and right panel—side view.

constant voltage of 40 V for 48 h. The electrolyte was vigorously stirred, and its temperature was kept between 2 and 4 °C. After the first anodization step the alumina film was selectively etched away in a mixture of 35 ml/l $H_3PO_4$ and 20 g/l $CrO_3$ at 70 °C. At this stage an ordered texture replicating the structure of the AAO pore bottoms was formed on the aluminum surface. Finally the foils were subjected to a second anodization process at the same conditions. To obtain films of different thickness the duration of the second anodization was varied from 3 to 72 h. Thus we obtained six samples of films with equal interpore distance (105 nm) and pore radius (20 nm), but with different thickness of 6, 12, 24, 50, 105, and 163 $\mu$m. Scanning electron microscopy (SEM) pictures shown in Fig. 1 were recorded on a Supra 50 VP instrument (LEO). The images show the standard quality of the structure of the obtained AAO films. Particularly, AAO films demonstrate extremely high degree of straightness and uniformity of depth of pores. It is provided by a technology of their synthesis. The spacing between pores are much poorly determined that produce significant degree of disorder in the plane of the film.

SANS measurements were carried out with a neutron beam ranging in a wavelength from $\lambda=0.5$ to 1.2 nm, with a wavelength spread of $\Delta\lambda/\lambda=0.1$ and a divergence $\eta=1.5$ mrad [SANS-2 at the Geesthacht Neutron Facility (GeNF)]. The films with an area of 1 $cm^2$ were oriented perpendicularly to the neutron beam (Fig. 2). At this orientation the pores are parallel to the incident neutron beam. The scattered neutrons were detected by a position sensitive detector with $256\times256$ pixels. The geometry chosen for the experiment allows to observe a diffraction pattern with a range as shown in Fig. 2. The obtained many-order reflection pattern suggests that strong correlations either in the pore positions or in the domain orientations exist over significant distances. The hexagonal arrangement of reflections demonstrates the sixfold symmetry along the direction normal to the film surface with a pore distance of 105 nm. The hexagonal arrangements of pores appear to have long-range correlation exceeding the sample despite being formed on polycrystalline aluminum. In fact the pore structure consists of short-range domains with the poor positional order of pores and with the size smaller than the polycrystals of aluminum. There is another, orientational order between these domains that can exceed the size of the aluminum polycrystals and this orientational, but not positional, correlation reaches as far as the size of the whole AAO film. It is believed that this

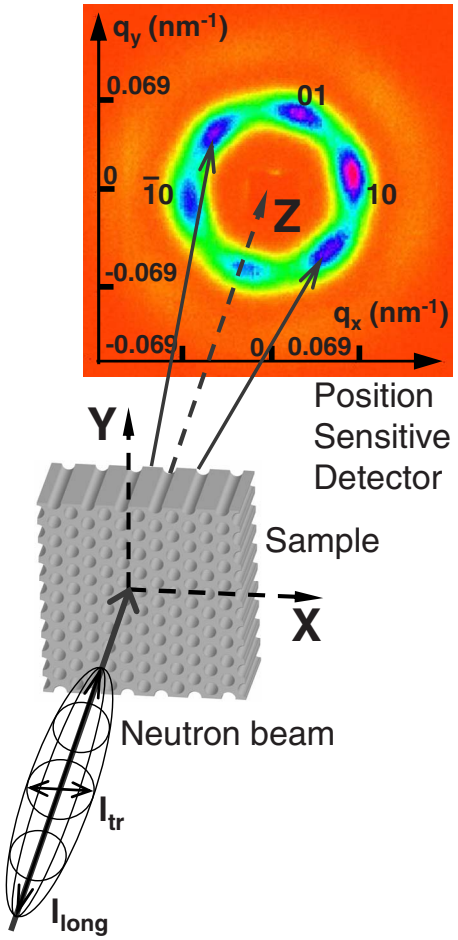


FIG. 2. (Color online) Schematic drawing of the experiment. A typical diffraction pattern obtained from AAO film with $L=24$ $\mu$m.

long-range orientational order stem from the incredibly high degree of straightness of pores provided by the technological processes.

### III. THEORETICAL BACKGROUND

To theoretically describe such an experiment, let us consider small-angle neutron scattering on a thin film with ordered identical pores. We assume that the pores have the shape of cylinders with axis perpendicular to the film plane and extend through the full film thickness. The centers of the pores form a perfect two-dimensional hexagonal lattice. We represent the coherent small-angle elastic neutron scattering as scattering on an effective potential $U(\mathbf{r})$ which is zero inside the pores and equal to the constant $E(1-n^2)$ in between. Here $E=(\hbar k)^2/(2m)$ is the neutron energy in vacuum and $n$ the refractive index,[19,20] determined by the scattering length density $\mathcal{B}=\Sigma_i\rho_i a_i$ via $n=1-(\lambda^2/2\pi)\mathcal{B}$. Here $\rho_i$ and $a_i$ are the density and the coherent scattering length of the atoms of type $i$, respectively. For slow neutrons $(1-n)$ depends on wavelength and is of order of $10^{-5}$–$10^{-6}$ for most materials.[19] Then, $E$ will be $\gg|U|$ and one has a process of small-angle scattering of high-energy particles. Following Ref. 20 and assuming that the neutrons travel along the $z$ axis

perpendicular to the film plane, we obtain the scattering amplitude

$$f_{\mathbf{Q}} = \frac{k}{2\pi i}\int d\boldsymbol{\rho}\,\exp(-i\mathbf{Q}\boldsymbol{\rho})\int dz\,\exp(-iQ_z z)\frac{dC(\boldsymbol{\rho},z)}{dz}, \tag{1}$$

where $\mathbf{Q}$ is the momentum transfer, with $Q_z=-Q^2/2k$,

$$C(\boldsymbol{\rho},z) = \exp\left(-\frac{im}{\hbar^2 k}\int_{-\infty}^{z} dz' U(\boldsymbol{\rho},z')\right), \tag{2}$$

and $\boldsymbol{\rho}$ is a vector in the plane of the film (see Fig. 2).

The integrals in Eqs. (1) and (2) can be easily taken. Apart from an insignificant phase factor we obtain

$$f_{\mathbf{Q}} = \frac{kR^2}{d_Q}\sin\left(\frac{kL(1-n)}{2}d_Q\right)F(Q)S(\mathbf{Q}), \tag{3}$$

$$d_Q = 1-\frac{Q^2}{2k^2(1-n)} = 1-\frac{Q^2}{4\pi\mathcal{B}}, \tag{4}$$

where $L$ is the film thickness, $R$ the pore radius, $J_1(x)$ the Bessel function of the first kind and the first order, and $kL(1-n)=\lambda L\mathcal{B}$. $S(\mathbf{Q})=\Sigma_n\exp(-i\mathbf{Q}\boldsymbol{\rho}_n)$ is the structure factor, where the summation is taken over the pore centers located at $\boldsymbol{\rho}_n$. $F(Q)=2J_1(QR)/(QR)$ is the form factor of a cylinder when the neutron propagation vector $\mathbf{k}$ is parallel to the cylinder axis. It should be noted that the factor $d_Q$ in Eq. (3) arises from the longitudinal component of the momentum transfer $Q_z$ in Eq. (1). Although the momentum transfer is often considered to be in two dimensions ($Q_z=0$) (Ref. 20) for $E \gg |U|$ [so that $d_Q=1$ in Eq. (3)], the component $Q_z$ is important for our discussion. For example, in our experiment $d_{Q_{10}}\approx 0.2$ but one could assume $d_{Q_{ij}}\approx 1$ for $Q_{ij}$ with $i,j \sim 1$ if the hexagonal lattice constant $a$ was larger than 300 nm.

Equation (3) can be rewritten in a simple form

$$f_{\mathbf{Q}} = V\mathcal{B}F(Q)S(\mathbf{Q})\frac{\sin x}{x}, \tag{5}$$

where $V=\pi R^2 L$ is the volume of the cylinder and the argument $x=kL(1-n)d_Q/2$. When $x\to 0$ so that the function $\sin(x)/x\to 1$, the Born approximation is valid in Eq. (5). However, if $x\geq 1$ it will be violated.[20] In the conditions of our experiment with $\langle\lambda\rangle=0.6$ nm and $(1-n_{Al_2O_3})\approx 3\cdot 10^{-5}$, already for a sample thickness as small as $L=10$ $\mu$m one has $\lambda L\mathcal{B}=\pi$. So this simple estimation shows that the Born approximation has a rather narrow applicability range: only for samples thinner than 10 $\mu$m.

Interestingly, neither the period of the structure determining the structure factor $S(\mathbf{Q})$, nor the pore radius $R$ directly influences the range where the Born approximation is valid. Furthermore, in accordance with Eqs. (3)–(5), extending $x$ beyond the Born approximation does not affect the structure factor. It stays, indeed, unchanged. The spatial scale of the structure, however, does play a role in our consideration. For example, if we can assume a pore as an ideal object (a cylinder), then the poorly determined spacing between pores does not affect the validity of Eqs. (1)–(3), since make transformed the structure factor only while prefactors, including form factor $F(Q)$ stay unchanged.

So far we used the plane-wave approximation and assumed that the scattered waves can be coherently added. In practice, the neutron beam has a limited coherence, hence interference can only take place between waves scattered within a limited sample volume. The coherence length of a neutron beam in transverse direction ($l_{tr}=\lambda/\eta$) is determined primarily by the "angular resolution" $\eta$ of the beam, i.e., its collimation.[8] For our setting $l_{tr}\approx 500$ nm, so the scattering of a single cylinder can interfere with only $N=(l_{tr}/a)^2\approx 25$ nearest cylinders out of $10^{10}$ inside the neutron beam. Cylinders at distances much larger than $l_{tr}$ are irradiated by neutron waves with different and uncorrelated phases. Still, the interference of a limited number of scattering cylinders can deplete the incident beam significantly, since the relatively low value of $l_{tr}/a$ can only affect the apparent width of the Bragg peaks in $S(\mathbf{Q})$, but not violate the Born approximation, which is solely determined by $\lambda L\mathcal{B}$.

The coherence length in the direction parallel to the beam $l_{long}=\lambda^2/\Delta\lambda$ is primarily determined by the spectral width $\Delta\lambda$ of the source[21] and in our case $l_{long}\approx 10$ nm. In a scattering experiment the difference in path length for neutrons scattered at the front and at the back side of a thin membrane of thickness $L$ is $2L\sin^2\theta_B$.[11] The coherence length should actually exceed this difference ($l_{long}>2L\sin^2\theta_B$) to provide the conditions within which the scattered waves are still able to interfere. This increases significantly the depth of the coherent volume to

$$L_{long} \leq \frac{l_{long}}{2\sin^2(\theta_B)} \sim \left(\frac{\lambda}{\Delta\lambda}\right)\frac{d^2}{\lambda}. \tag{6}$$

Here we used Bragg's law to substitute $\sin\theta_B\to\lambda/2d$, where $d$ is the interplane distance. Thus, in small-angle diffraction the coherence length is inversely proportional to the neutron wavelength $\lambda$ and in our case is estimated to be smaller than 50–100 $\mu$m. At such large longitudinal coherence length the parameter $\lambda L\mathcal{B}$ can be significant, so that the diffraction can switch into the strong wave-sample coupling regime far beyond the Born approximation. Generally speaking, there may be other contributions in the rocking curve[22] but as will be shown below they are not important for our consideration.

The longitudinal coherence length in our experiment can be directly measured by the variation in the scattered intensity with $Q_z$, i.e., as a function of the rocking angle of the sample toward the incident beam. This rock will carry the $(xy)$ plane of $Q$ space through the Ewald sphere. The width of the rocking curve $\delta$ is related to the coherence length $L_z$ via

$$L_{z,exp} = \frac{2\pi}{\Delta Q_z} = \frac{2\pi}{Q_{10}\sin\delta}. \tag{7}$$

If the longitudinal coherence length of the beam $L_{long}$ exceeds the length of the pores $L$, the coherence length $L_{z,exp}$ found in the experiment will be equal to the coherence length of the sample, i.e., the pore length $L$. Vice versa, if $L_{long}$ is shorter than the length $L$ of the pores, $L_{z,exp}$ will be equal to

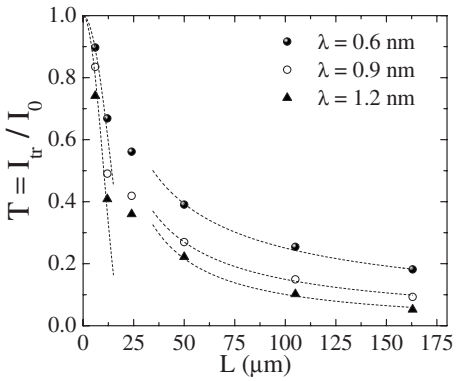


FIG. 3. The transmission of the beam through the membrane $T$ as a function of the AAO film thickness for different neutron wavelengths $\lambda=0.6$, 0.9, and 1.2 nm. The dashed lines in the range of small $L$ are quadratic dependences of transmission with the thickness $T=I_{tr}/I_0=1-\alpha^2L^2$, with $\alpha^{-1}\sim 12-18$ $\mu$m. The dashed lines in the range of large $L$ are the power-law dependences ($\sim L^{-x}$ with $x\sim 1$) (see the text).

the coherence length of the neutron beam $L_{long}$, which depends on $\lambda$ [Eq. (6)]. It should be noted that the parameter $L$ in Eqs. (3) and (5) for the case of the experiment must be taken equal to $L_{z,exp}$ as measured in the rocking scan of the corresponding Bragg reflection.

## IV. RESULTS

The first surprising feature is the incredibly high scattering power of the AAO membranes. Figure 3 shows the transmission through the membranes of different thickness: $T=I_{tr}/I_0$, where $I_0$ and $I_{tr}$ are the intensities of the incident and transmitted (nonscattered) beam, respectively. Already for samples of thickness 10–20 $\mu$m half the incident intensity is scattered. This is not yet an indication that the scattering goes beyond the Born approximation, but it is a hint that the incident wave has a very strong interaction with the sample. For comparison, a standard sample for a SANS experiment is prepared at a thickness of 1 mm in order to scatter 10% of the incident beam. Our membranes scatter 10 times more neutrons, in spite of the fact that they are 100 times thinner.

The second features are the measured rocking curves to determine the longitudinal coherence length. Rocking scan experiments were carried out by rotating the films around the $Y$ axis (see Fig. 2) over a range of 5° with a step of 0.1° at wavelengths of the neutron beam $\lambda=0.6$, 0.9, and 1.2 nm, so that one observes the appearance, enhancement and weakening of the 10 and $\bar{1}0$ reflections on the $q_x$ axis. As an example Figs. 4(a) and 4(b) give the curves for the samples with $L=6$ and 24 $\mu$m, respectively. These curves are fitted with a Lorentzian with the width $\delta$, position $\alpha_{1,2}$, and integral amplitude $A_{int}$ of the rocking curve as parameters. The wavelength dependence of the width $\delta$ for the same samples is shown in Fig. 5. It is interesting that $\delta$ does not change with wavelength for the thin AAO membrane with $L=6$ $\mu$m. The longitudinal coherence length $L_{z,exp}$ calculated using Eq. (7) is equal to 5.95, 6.14, and 6.26 $\mu$m for wavelengths $\lambda=0.6$, 0.9, and 1.2 nm, respectively. The integral amplitude $A_{int}$

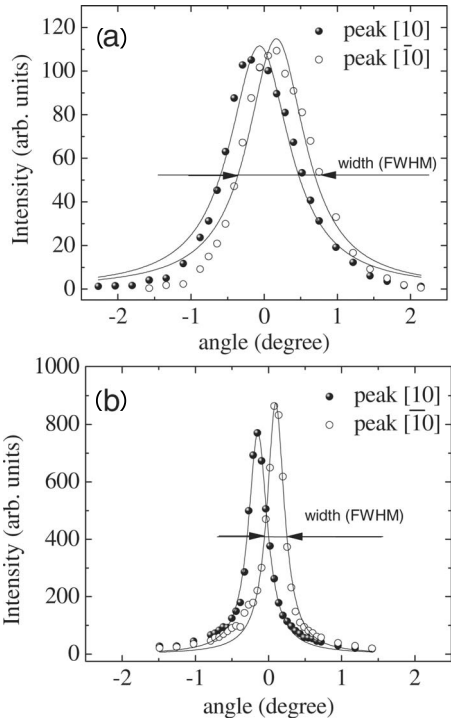


FIG. 4. The rocking curve of 10 and $\bar{1}0$ reflections for the samples with thickness (a) 6 $\mu$m and (b) 24 $\mu$m.

slightly increases with wavelength. In contrast, for the thick membrane with $L=24$ $\mu$m, the width $\delta$ linearly increases with $\lambda$ (Fig. 5). The coherence length is equal to $L_{z,exp}=19$, 12.59, and 9.99 $\mu$m for $\lambda=0.6$, 0.9, and 1.2 nm, respectively. The integral amplitude $A_{int}$ decreases strongly with wavelength.

Thus, one concludes that for the thin membrane the coherence length of the beam $L_{long}$ exceeds the length of the pores $L$ and, therefore, $\delta$ corresponds to the inverse coherence length of the sample, equal to the length of the pores. On the other hand, the coherence length of the thick sample remains unknown, but $\delta$ corresponds to the beam coherence and can be described by Eq. (6).

The third feature showing the importance of the coherence of the neutron beam is the wavelength dependence of the scattered intensity. The momentum-transfer dependence of the scattered intensity $I(q)/I_0$ (normalized to the incident

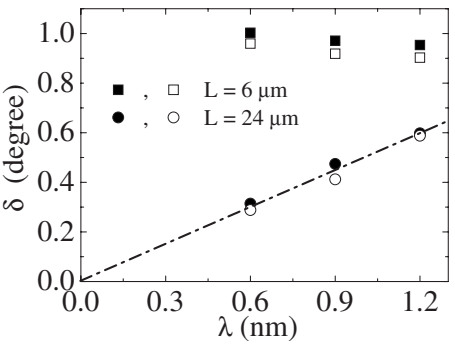


FIG. 5. Wavelength dependence of the rocking curve width $\delta$ (FWHM) for the samples with thickness 6 $\mu$m and 24 $\mu$m.

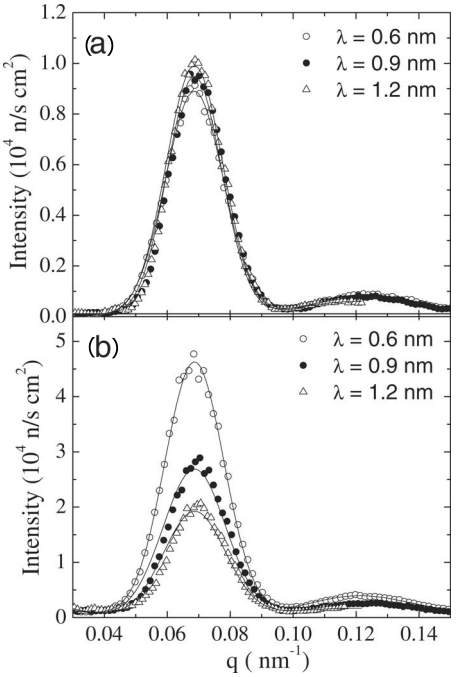


FIG. 6. The momentum-transfer dependence of the neutron scattering for the sample with (a) $L=6$ $\mu$m and (b) $L=24$ $\mu$m for different neutron wavelengths $\lambda=0.6$, 0.9, and 1.2 nm.

intensity), with the wave-vector transfer **Q** parallel to the (10) axis, for the samples with $L=6$ and 24 $\mu$m is shown in Figs. 6. It is seen in Fig. 6(a) that for the thin sample ($L=6$ $\mu$m) the scattered intensity for three different wavelengths λ is independent of λ. However, for the thick sample ($L=24$ $\mu$m) the amplitude of the scattering decreases strongly when λ is increased, as seen in Fig. 6(b). The $q$ dependence can be satisfactorily reproduced by a sum of Gaussians with centers at $Q_{10}=0.069\pm0.004$ nm$^{-1}$, $Q_{11}=0.119\pm0.004$ nm$^{-1}$, and $Q_{20}=0.138\pm0.004$ nm$^{-1}$, which are well classified in the hexagonal lattice with the parameter $a=105\pm2$ nm. The width of the reflections is described by a half-width at half maximum $\omega(\sim 1/l_{\mathrm{tr}})=0.0100\pm0.0005$ nm$^{-1}$ which can be attributed to the resolution of the setup. The whole set of experimental data for different λ and different thickness $L$ was fitted with combinations of Gaussians as described above with the amplitude of the scattering as the only variable parameter.

The λ dependence of intensity of the (10) peak is shown in Fig. 7 for samples with various thickness. As is well seen the amplitude is small and independent of λ for $L=6$ $\mu$m. For samples with higher thicknesses $L$, the peak intensity decreases with increase in the wavelength. The λ dependence of the intensity for the thick samples is close to the power-law $\sim\lambda^{-2}$ that is shown in Fig. 7 by the dashed line. This wavelength dependence of the scattering intensity is clearly related to the change in the longitudinal coherence length $L_{\mathrm{long}}$ observed experimentally (Fig. 5) and predicted by Eq. (6). In fact the limited value of the coherence length restricts the possibility to observe the transition from scattering within the Born approximation (for the thin sample) to scattering in the regime beyond its applicability (for the thick samples).

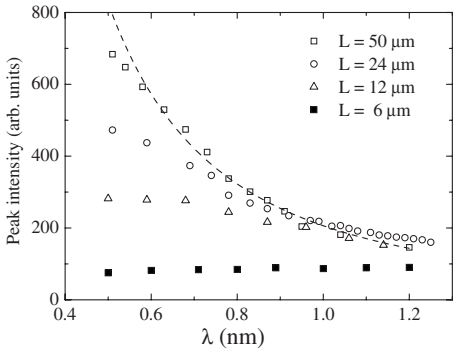


FIG. 7. Wavelength dependence of the peak (10) intensity for different thickness of the AAO films $L=6$, 12, 24, and 50 $\mu$m.

It is worthy to note that we do not correct for the extinction in the treatment of the data above because such correction has a limited applicability in given case. This question is not trivial and requires some discussion. There are several sources for extinction: absorption, incoherent scattering, and multiple scattering. The first and the second sources can be ignored for sample of Al2O3 with the thickness less than 100 mkm. The multiple (double, etc.) scattering may occur in the sample considering very strong scattering power of the pore system. The multiple scattering enhances under the following conditions: the sample is relatively thick, thicker than the coherent scattering length (either the coherent length of radiation, or the coherent length of the scattering object itself). In this paper we estimated these coherent lengths be larger or of order of 20–25 mkm. Therefore, the extinction related to the multiple scattering should be taken into account for the samples thicker than 20–25 mkm. The purpose of this paper is to describe the single scattering event occurring in such system, that is why we concentrate on the samples with thickness of 6, 12, 24 mkm. Thus we believe that these three samples can be treated without correction for the extinction as soon the scattering can be considered as a single scattering event. The thicker samples should be treated accounting for extinction due to multiple scattering but those data are not really included in the paper.

To summarize, it is the "ellipsoid"-like shape of the coherent volume (Fig. 2) that allows to significantly enhance the diffraction effects from $2d$ periodical nanostructures with a third ultimately large nonperiodic dimension. A sweet marriage between the objects under study and our method (SANS) is apparent in the high scattering power of the AAO films (Fig. 3). For thin films ($L=6$ and 12 $\mu$m) the Born approximation is more or less applicable. In this case the intensity of the diffracted waves grows quadratically with sample thickness, hence the transmission $T=I_{\mathrm{tr}}/I_0=1-\alpha^2L^2$ falls off quadratically, where $\alpha^{-1}\sim 12-18$ $\mu$m for different neutron wavelengths. The applicability of the Born approximation is confirmed by the wavelength-independent neutron scattering amplitude as shown in Figs. 6(a) and 7 for the AAO film with $L=6$ $\mu$m. According to the predictions in [Eqs. (3)–(5)], for thicker samples the Born approximation is no more valid. However, the expected sinus-square dependence on the argument $\lambda L\mathcal{B}/2$ [Eq. (3)] was not observed, neither in the thickness dependence of the transmission (Fig.

3) nor in the wavelength dependence of the peak intensity (Fig. 7). Instead, the $T(L)$ decay changes to a slow power-law dependence ($\sim L^{-x}$ with $x \sim 1$) at large $L$ that should be rather attributed to multiple scattering. Additionally for thicker samples the scattering intensity is proportional to $\lambda^{-2}$. The difficulties to observe the expected oscillating behavior of the scattering intensity stem from the finite longitudinal coherence of the beam. Thus, one concludes that the example of scattering in AAO films can be described by the theoretical model [Eqs. (3) and (5)] taking into account the coherency in the both used radiation and parameters of the investigated object.

## V. CONCLUDING REMARKS

Although the above consideration is carried out for neutron scattering, Eqs. (1)–(5) could be applied for the photon scattering with wavelength $\lambda \sim 1$ Å, with $U=(\hbar k)^2 (1-n^2)/(2m)$ between pores and $U=0$ inside them as it was considered for neutrons. Naturally, the meaning of $U$ in Eq. (2) for neutron and for photon is different and we have here only the quantitative coincidence of the scattering amplitudes for neutron and photon. Equations (1) and (2) give the photon scattering amplitude in the Hulst approximation, which was proposed originally for scattering on a sphere and which works well when the sphere radius $R \gg \lambda$ and $|1-n| \ll 1$ (see Ref. 23). Expanding the sine in Eq. (3) up to the first term we obtain the scattering amplitude for small scattering angles within the Rayleigh-Gans approximation (with the magnetic permeability equal to unity), which is the analog of the Born approximation in quantum mechanics.[23] The refraction coefficients for slow neutron and photon with $\lambda \sim 1$ Å lay in the same interval $(1-n) \sim 10^{-5}$–$10^{-6}$ in the majority of materials. This makes quantitative estimations for slow neutron presented above to be valid also for photon.

The small-angle neutron diffraction on the vortex lattice in superconductors or the ordered system of magnetic nanowires can possess the same intriguing features. However, for the reason of the complex spatial distribution of the magnetic flux an exact theoretical solution in this case is difficult to derive in a simple analytical way. Yet such calculations can be appropriate to describe scattering from flux lines in superconductors on the qualitative level. In niobium, the "field contrast" between the flux line cores and the field minima between them is of order of 100–200 mT at low temperatures. For neutrons of wavelength 1.0 nm, this gives a refractive index difference of order of $10^{-5}$. Hence, the deviation from Born approximation (a phase difference accumulated along the flux line cores of order $\pi$) will occur along a length $L \approx 50$ $\mu$m. To observe scattering beyond the Born approximation will require the length of the neutron coherence volume (and the length over which the flux lines are straight) to exceed $L$. Hence the observation of this effect in flux lines is possible for niobium but can be rather impossible in high-Tc or heavy-fermion superconductors, which have much smaller values of the field contrast. The detailed analysis of the situation should wait until the corresponding experiments are performed.

To conclude with, the paper presents the exact theoretical solution describing the small-angle diffraction from a nanostructure with two periodic and one nonperiodic dimensions. It was shown that the coherency of the standard SANS setups suits ideally to the geometry of the objects under study. The theory had been tested with the example of scattering on AAO films. It is pointed out that this consideration may have a significant impact on the diffraction experiments on Abrikosov's flux lines in superconductors. We emphasize that intensity of the scattering is strongly affected by the coherency and the wavelength of the used radiation.

## ACKNOWLEDGMENTS

The PNPI teams acknowledge GKSS for hospitality. This work was performed within the framework of a Federal Special Scientific and Technical Program (Projects No. 02.513.11.3392 and No. 02.513.11.3485). Russian authors thank for partial support the Russian Foundation of Basic Research (Grant No. 10-02-00634).

[1] H. Pan, B. Liu, J. Yi, C. Poh, S. Lim, J. Ding, Y. Feng, C. H. A. Huan, and J. Lin, J. Phys. Chem. B **109**, 3094 (2005).
[2] K. Nielsch, F. Muller, and A. P. Li, Adv. Mater. **12**, 582 (2000).
[3] K. S. Napolskii, P. J. Barczuk, S. Yu. Vassiliev, A. G. Veresov, G. A. Tsirlina, and P. J. Kulesza, Electrochim. Acta **52**, 7910 (2007).
[4] O. Jessensky, F. Muller, and U. Gosele, J. Electrochem. Soc. **145**, 3735 (1998).
[5] F. Li, L. Zhang, and R. M. Metzger, Chem. Mater. **10**, 2470 (1998).
[6] H. Masuda, F. Hasegwa, and S. Ono, J. Electrochem. Soc. **144**, L127 (1997).
[7] K. Nielsch, J. Choi, K. Schwirn, R. B. Wehrspohn, and U. Gösele, Nano Lett. **2**, 677 (2002).
[8] R. E. Benfield, D. Grandjean, J. C. Dore, H. Esfahanian, Z. Wu, M. Kröll, M. Geerkens, and G. Schmid, Faraday Discuss. **125**, 327 (2004).
[9] H. Versmold, Phys. Rev. Lett. **75**, 763 (1995).
[10] W. L. Vos, M. Megens, C. M. van Kats, and P. Bosecke, Langmuir **13**, 6004 (1997).
[11] A. V. Petukhov, D. G. A. L. Aarts, I. P. Dolbnya, E. H. A. de Hoog, K. Kassapidou, G. J. Vroege, W. Bras, and H. N. W. Lekkerkerker, Phys. Rev. Lett. **88**, 208301 (2002).
[12] B. J. Lemaire, P. Davidson, J. Ferré, J. P. Jamet, P. Panine, I. Dozov, and J. P. Jolivet, Phys. Rev. Lett. **88**, 125507 (2002).
[13] A. V. Petukhov, D. van der Beek, R. P. A. Dullens, I. P. Dolbnya, G. J. Vroege, and H. N. W. Lekkerkerker, Phys. Rev. Lett. **95**, 077801 (2005).
[14] E. M. Forgan, D. M. Paul, H. A. Mook, P. A. Timmins, H. Keller, S. Sutton, and J. S. Abell, Nature (London) **343**, 735 (1990).
[15] A. D. Bianchi, M. Kenzelmann, L. DeBeer-Schmitt, J. S. White, E. M. Forgan, J. Mesot, M. Zolliker, J. Kohlbrecher, R.

Movshovich, E. D. Bauer, J. L. Sarrao, Z. Fisk, C. Petrovic, and M. R. Eskildsen, Science **319**, 177 (2008).
[16] A. Huxley, P. Rodiere, D. McK. Paul, N. van Dijk, R. Cubitt, and J. Flouquet, Nature (London) **406**, 160 (2000).
[17] H. Masuda and K. Fukuda, Science **268**, 1466 (1995).
[18] S. Shingubara, J. Nanopart. Res. **5**, 17 (2003).
[19] V. F. Sears, *Neutron Optics* (Oxford University Press, Oxford, 1989).
[20] L. D. Landau and E. M. Livshitz, *Quantum Mechanics* (Pergamon, Oxford, 1977).
[21] M. Born and E. Wolf, *Principles of Optics* (Pergamon Press, Oxford, 1970).
[22] R. Cubitt, E. M. Forgan, D. McK. Paul, S. L. Lee, J. S. Abell, H. Mook, and P. A. Timmins, Physica B **180-181**, 377 (1992).
[23] R. G. Newton, *Scattering Theory of Waves and Particles*, 2nd ed. (Dover Publications, New York, 2002).